Progress In Electromagnetics Research C, Vol. 110, 197–212, 2021

Dynamically Switched Dual-Band Dual-Polarized Dual-Sense Low-Profile Compact Slot Circularly Polarized Antenna Assisted with High Gain Reflector for Sub-6 GHz and X-Band Applications

Asutosh Mohanty[1, *] and Bikash R. Behera[2]

Abstract—A low-profile compact uni-planar slot antenna design of size 26 mm × 26 mm is proposed, assisted with a metallic bottom reflector at a height of $\frac{\lambda}{6}$ (λ is the lowest CP frequency). The dual-band dual-polarization is observed at 6.2 GHz and 9.3 GHz, and polarization sense (LHCP and RHCP) is dynamically switched by introducing a pair of RF p-i-n diodes mounted at the confluence of right-slot (RS) and left-slot (LS). A metallic reflector of size 60 mm × 60 mm helps to improve overall impedance matching, enhance antenna gain and assertsq uni-directional dual-polarized radiation with good back-lobe suppression. The proposed antenna operates at dual bands (5.46–6.76 GHz) with 21.27% IBW and (8.18–10.48 GHz) with 24.65% IBW for $S_{11} < -10$ dB. The antenna gain reaches (7.82–8.75 dBi) for D1-OFF, D2-ON state with (9.2%, 15.63%) axial bandwidths and (6.42–7.0 dBi) for D1-ON, D2-OFF state with (7.53%, 16.04%) axial bandwidths with radiation efficiency ranging (75%–87%). A prototype antenna is fabricated and measured, which shows good agreements with simulated performances and can be used for sub-6 GHz in 5G applications and X-band radar systems.

1. INTRODUCTION

In present scenario, circularly polarized (CP) antennas are often considered as an important part for highly demanded sub-6 GHz band for 5G applications and X-band radar systems [1, 2]. To satisfy such a requirement, dynamically switched CP antennas are adopted for improving polarization attributes, bringing system and wireless diversity to a platform, where system capacity can be improved with compensation to fast fading effects in radio channels. To provide improved wireless link at relatively low cost, dual-band dual-polarized dual-sense antennas have superior performances in terms of polarization purity in which orthogonal E-field components boost the overall RF performance by compensating polarization mismatch losses. Moreover, the polarization characteristics can be dynamically switched, depending on users' RF requirements [3, 4].

In [5], a dual-sense CP patch antenna is designed using a dual-coupled line, with gains 5.3/5.7 dBi. Utilizing a capacitive-probe method, a dual-band dual-mode dual-polarized patch antenna is achieved in [6], with two mode antenna gains 1.1/8.4 dBi. For BeiDou navigation satellite applications, [7] designs a dual-band dual-polarized annular-ring CP antenna with gain variation of 4.3/6.4 dBi at dual bands. A bow-tie shaped dual-band dual-polarized antenna with integrated electric dipole and metal cavity as a magnetic dipole connected to an array resonator is designed in [8], with dual band gains of 4.2/6.3 dBi. A cross dipole structure CP antenna with dual-band dual-sense characteristics is achieved in [9] for WLAN/Wi-MAX applications with dual band gains of 7.7/7.4 dBi. In [10], a dual-band dual-polarized antenna with less radiating layers, only one layer radiating patch, is achieved with a dual band gains

Received 5 January 2021, Accepted 23 February 2021, Scheduled 3 March 2021
* Corresponding author: Asutosh Mohanty (asutoshmohanty.kiit0409@gmail.com).
[1] School of Electronics Engineering, KIIT Deemed to be University Bhubaneswar, Odisha 751024, India. [2] Advanced RF and Microwave Lab, Department of Electronics and Telecommunication Engineering, IIIT Bhubaneswar, Odisha 751003, India.

of 6.8/7.1 dBi. Integrating an SIW cavity in a bow-tie slot antenna dual band gains of 6.1/5.4 dBi with dual-band dual-polarized characteristics is achieved in [11]. In [12], a U-slot patch with four sequentially rotated shorted monopoles of a CP antenna is designed to achieve dual-band dual-mode with gains 0.8/6.8 dBi is achieved for GPS applications. A simple compact dual-band square slot antenna with dual-sense CP radiation for WLAN/Wi-Fi applications is discussed in [13], with dual band gains 4.2/3.4 dBi. In [14], using an open-end coplanar waveguide with an inverted L-structure fed to square slot is designed for a dual-band CP antenna for GPS and RFID applications with dual band gains 3.8/4.29 dBi. Considering the need of RF front-ends in WLAN/Wi-Fi/X-band radar applications [15–26], the trade-offs from the design point of view must be achieved using implicit techniques [27–31] before its validation for getting optimum antenna performances.

Inspired from the dual-band dual-polarized/dual-band dual-sense antenna designs of aforementioned reported articles, we propose a dual-band dual-polarized dual-sense uni-planar slot CP antenna, which is compact and has low profile, and its polarization sense (LHCP and RHCP) can be dynamically switched. Since this antenna is specifically designed for high gain and polarization diversity, much attention has been focussed on meeting the requirements for potential 5G applications in sub-6 GHz band and X-band radar systems. According to the authors' knowledge, antennas for dual-band dual-polarized dual-sense antenna at higher frequency applications with polarization sense switching mechanism have not yet been publicly addressed. The important aspects of antenna design are highlighted in the end.

2. ANTENNA DESIGN CONCEPTION AND WORKING MECHANISM

The proposed antenna consists of two parts. The first part is a uni-planar slot antenna of size $L_S \times W_S$ printed on a low-cost FR-4 substrate (thickness = 1.6 mm, $\varepsilon_r = 4.3$, $\tan\delta = 0.02$), and the second part consists of a metallic reflector of size $L_R \times W_R$ which is connected to the bottom part of antenna with supporting posts with an effective height h_e. The projection and side views are shown in Figure 2(a) and Figure 2(b), respectively. The antenna radiator section consists of a main slot (MS), which has been structurally made affline and two extended slots which are etched as right slot (RS) and left slot (LS) as shown in Figure 2(c). Two RF p-i-n diodes D1, D2 are mounted at the confluence of MS, RS, and LS, and this position is best fixed to reconfigure switching characteristics. Opposite diagonals are chamfered to improvise axial ratios at CP bands. The antenna is excited by a 50 Ω coaxial connector fed diagonally near MS.

The antenna design conception is analyzed from a cross-shaped (+) slot configuration in a square patch shown in Figure 1(a), generates orthogonal current modes (E° and E^{90} components) that triggers CP [32], hence we modifies (+) slot shape to affline slot configuration in which the slots are non-uniformly etched, as shown in Figure 1(b). This increases the electrical length due to self-asymmetry in slot geometry, and current path is changed. The antenna design architecture and reconfigurable polarization technology are motivated from [33–35] due to simple biasing structure, polarization strategy, and performances. The working principle of antenna is based on the excitation of MS slot which is

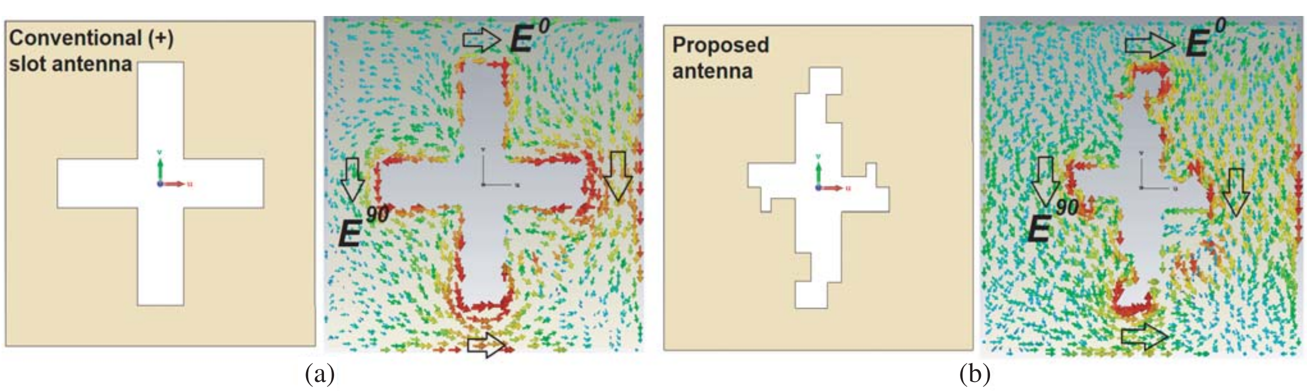

Figure 1. Current distributions in (a) Conventional (+) slot antenna, (b) Proposed slot antenna.

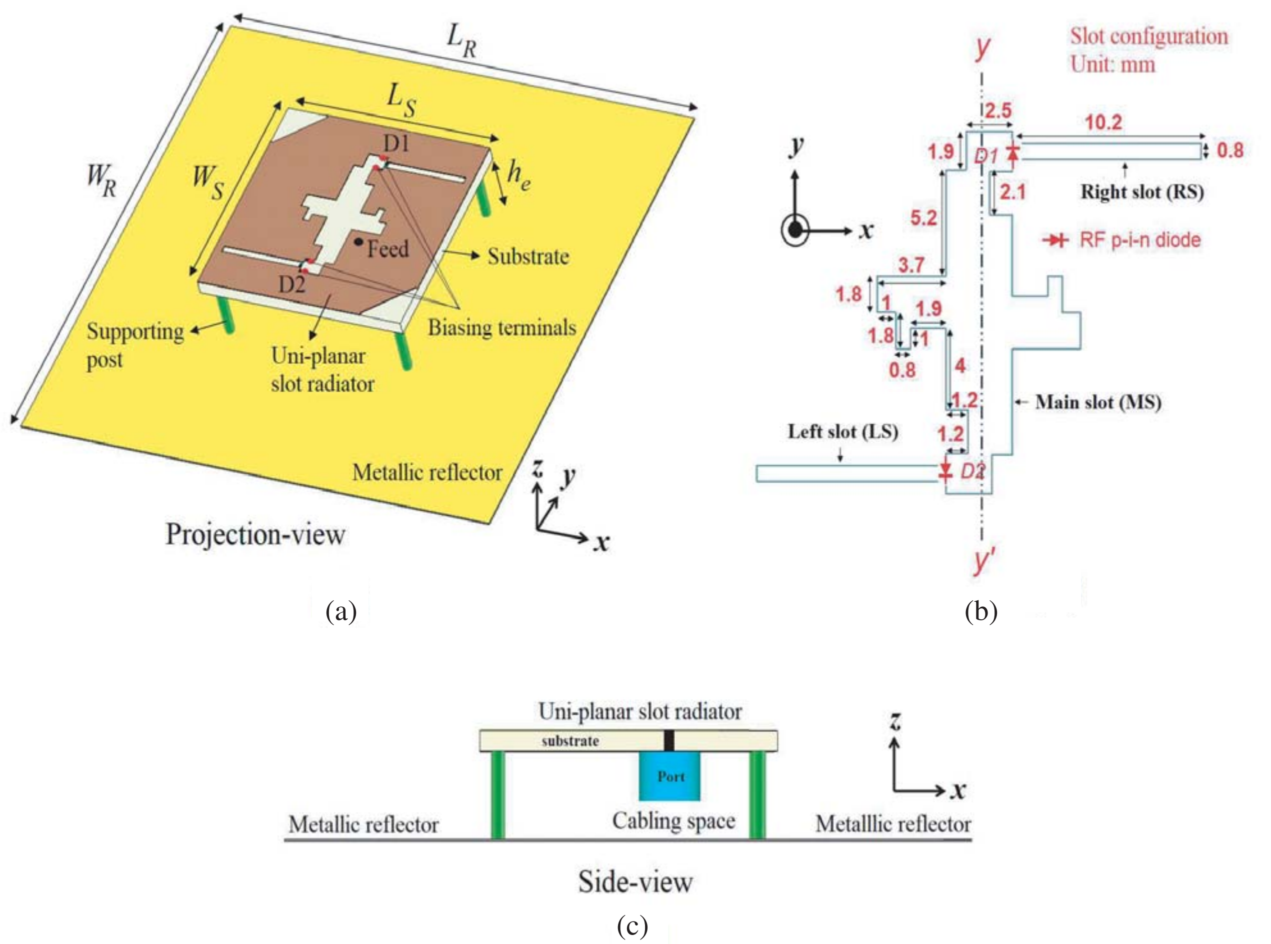

Figure 2. (a) Projection view. (b) Side view. (c) Slot configuration. Optimized antenna design parameters are: $L_S = 26\,\text{mm}$, $W_S = 26\,\text{mm}$, $L_R = 60\,\text{mm}$, $W_R = 60\,\text{mm}$, $a = 7\,\text{mm}$, $b = 3.7\,\text{mm}$, $h_e = 8.06\,\text{mm}$.

electrically/capacitively coupled to an inductively loaded patch. By stimulating the slot capacitance, the current oscillations in the constricting slots are disturbed. Hence, RF p-i-n diodes are mounted, which electrically shunt the magnetically coupled patch to polarize current oscillations in predefined reactive slots (MS, RS, and LS, respectively). (Note: — The initial attempts are investigated for choosing low-loss substrate, i.e., Rogers 5880, but it results in poor return loss, shifts in resonances and low gain characteristics. Hence, FR-4 (low-cost) substrate [36] is considered, to compensate the above stated deficiencies.)

The biasing circuit shown in Figure 3(a) and lumped switching circuit shown in Figure 3(b) consist of two RF p-i-n diodes *D1* and *D2* (Model: SMP 1320-079LF) mounted on the interface of MS, RS, and LS to assist switched polarization working modes. D.C. voltage supply (3 V, Max.) is provided through biasing pads. RF-blocking signal entry in the biasing lines has 27 nH inductors (*Model: AISC 0805-R027J-T*, 4nos, *L1, L2, L3, L4*, respectively). To protect diodes from D.C. voltage, 100 pF capacitors (*Model: Multicomp MC0402B101M500CT*, 2nos, *C1* and *C2*) are connected through conductive pads. The switching electrical parameters for ON or OFF states are considered as per the specifications in datasheet of standard packaging Skyworks RF p-i-n diode. For ON-state, $L_S = 0.7\,\text{nH}$, $R_S = 2\,\Omega$ are connected in series (draws an current $I_F = 1\,\text{mA}$), and for OFF-state, $L_S = 0.7\,\text{nH}$ is in series with parallel-fed $R_P = 10\,\text{K}\Omega$, $C_T = 0.23\,\text{pF}$. A CST-MWS EM-solver is used for simulating our antenna model, and switching model simulation is shown in Figure 3(c). In order to understand the switched polarization working modes of proposed antenna, surface current streamlines are vividly investigated.

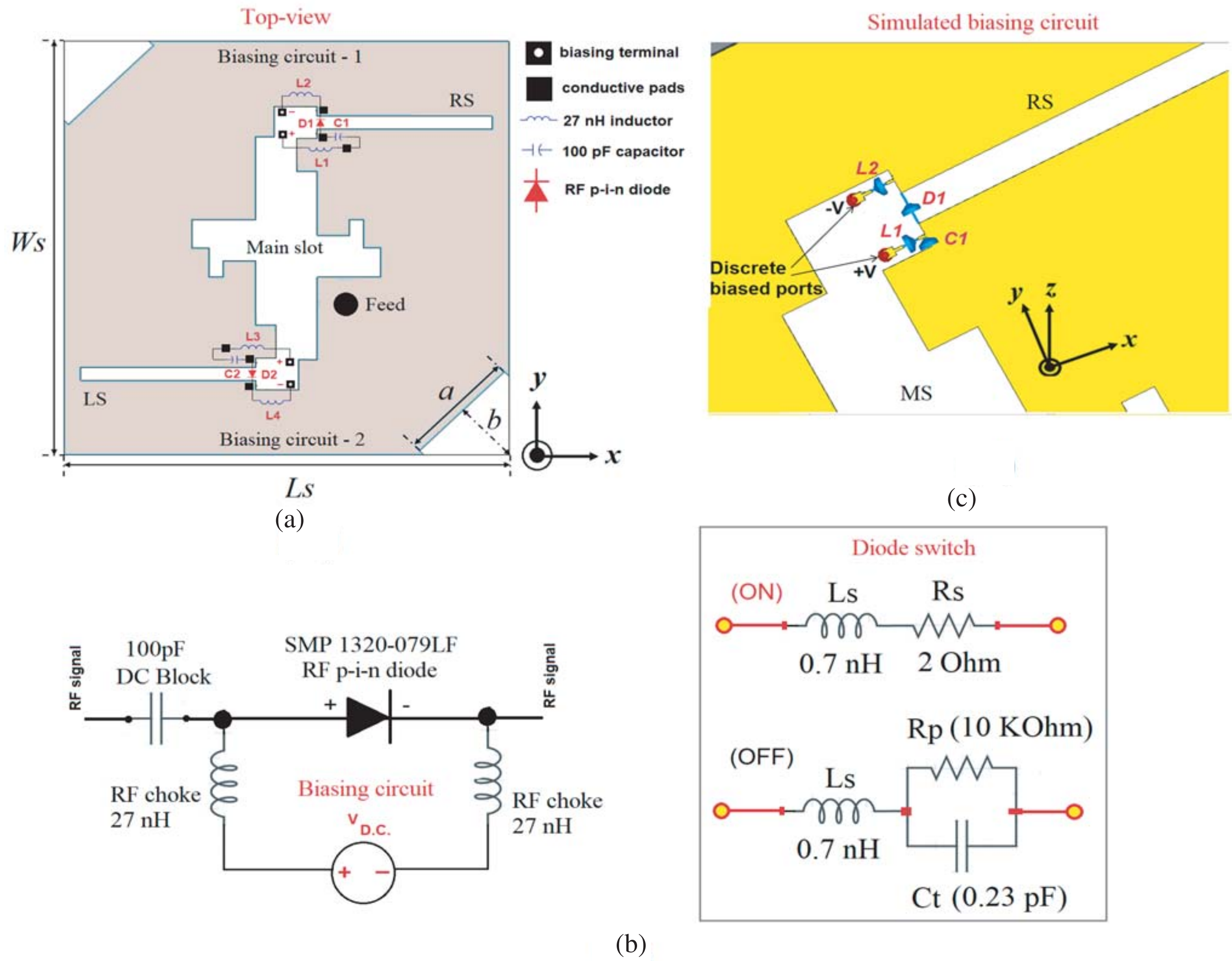

Figure 3. (a) Top view of antenna circuit. (b) Biasing circuit configuration and switching mechanism. (c) Simulated biasing circuit.

3. SURFACE CURRENTS ANALYSIS

Figure 4 shows the routing of current streamlines for D1-OFF, D2-ON state at $\omega t = 0°$ and $\omega t = 90°$ for dual bands. The vector rotation of currents in our proposed design shows CP patterns. It is observed, at 6.2 GHz for $\omega t = 0°$, that the current trace is clockwise, and for $\omega t = 90°$, the current trace is anticlockwise. Similarly, at 9.3 GHz for $\omega t = 0°$, the current trace is anticlockwise, and for $\omega t = 90°$, the current trace is clockwise. Hence, resultant current has a complementary phase rotation. Table 1 depicts the surface current magnitudes and CP characteristics for D1-OFF, D2-ON state.

Table 1. Surface current magnitudes and CP behaviour for D1-OFF, D2-ON state.

Frequency	ωt (deg.)	Surface current mag.	CP behaviour	Current rotation
6.2 GHz	$\omega t = 0°$	$J_{res}{}^{0} = J_{C1} + J_{C2}$	LHCP	Clockwise (↻)
6.2 GHz	$\omega t = 90°$	$J_{res}{}^{90} = J_{A1} + J_{A2}$	RHCP	Anti-clockwise (↺)
9.3 GHz	$\omega t = 0°$	$J_{res}{}^{0} = J_{A1} + J_{A2}$	RHCP	Anti-clockwise (↺)
9.3 GHz	$\omega t = 90°$	$J_{res}{}^{90} = J_{C1} + J_{C2}$	LHCP	Clockwise (↻)

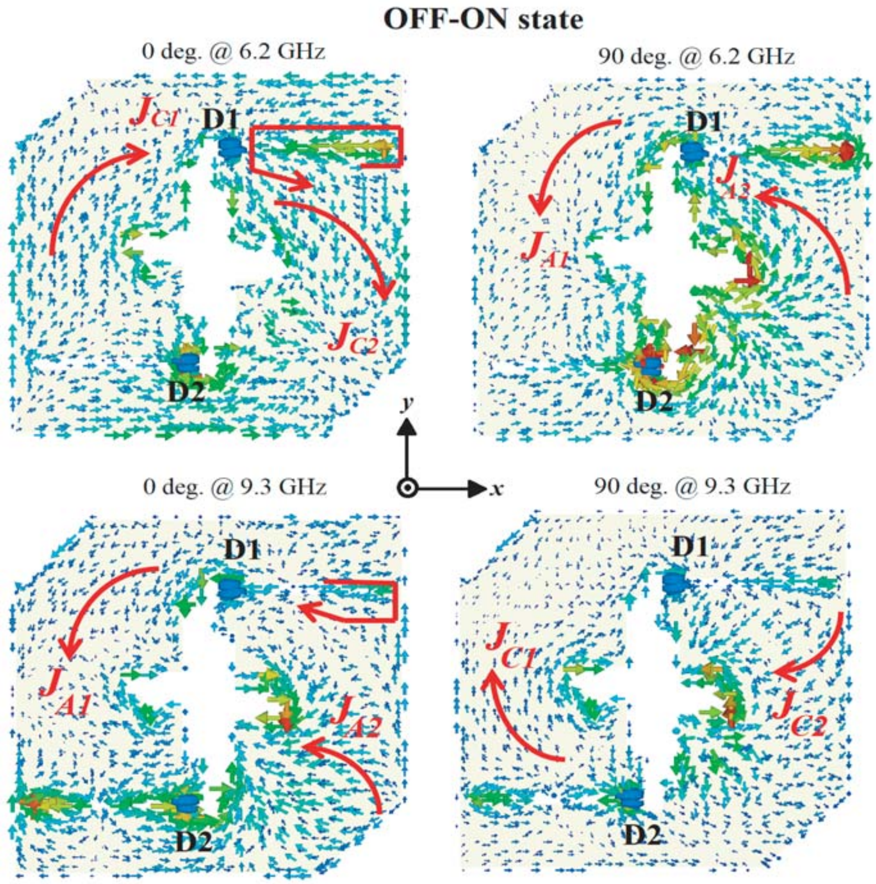

Figure 4. Surface current streamlines at 6.2 GHz and 9.3 GHz for D1-OFF, D2-ON state.

Similar contrast is observed in Figure 5, which shows the routing of current streamlines for D1-ON, D2-OFF state at $\omega t = 0°$ and $\omega t = 90°$ for dual bands. It is observed, at 6.2 GHz for $\omega t = 0°$, that the current trace is anticlockwise, and for $\omega t = 90°$, the current trace is clockwise. At 9.3 GHz for $\omega t = 0°$, the current trace is clockwise, and for $\omega t = 90°$, the current trace is anticlockwise. Hence, resultant current has complementary phase response. Table 2 depicts the surface current magnitudes and CP characteristics for D1-ON, D2-OFF state. From the above analysis, it is confirmed that the proposed antenna asserts dual-polarized dual-sense characteristics at dual bands.

Table 2. Surface current magnitudes and CP behaviour for D1-ON, D2-OFF state.

Frequency	ωt (deg.)	Surface current mag.	CP behaviour	Current rotation
6.2 GHz	$\omega t = 0°$	${J_{res}}^0 = J_{A1} + J_{A2}$	RHCP	Anti-clockwise (↺)
6.2 GHz	$\omega t = 90°$	${J_{res}}^{90} = J_{C1} + J_{C2}$	LHCP	Clockwise (↻)
9.3 GHz	$\omega t = 0°$	${J_{res}}^0 = J_{C1} + J_{C2}$	LHCP	Clockwise (↻)
9.3 GHz	$\omega t = 90°$	${J_{res}}^{90} = J_{A1} + J_{A2}$	RHCP	Anti-clockwise (↺)

The simulated S-parameters of proposed antenna for different biasing states (D1-OFF, D2-ON and D1-ON, D2-OFF) responses are shown in Figure 6(a). The improvement in the axial-ratio (dB) with diagonal edges on the antenna top surface is shown in Figure 6(b). The initial (+) slot on antenna generates CP behaviour, but 3-dB AR is slightly improved. When diagonal edges are chamfered, 3-dB ARs are much improved in both biasing states.

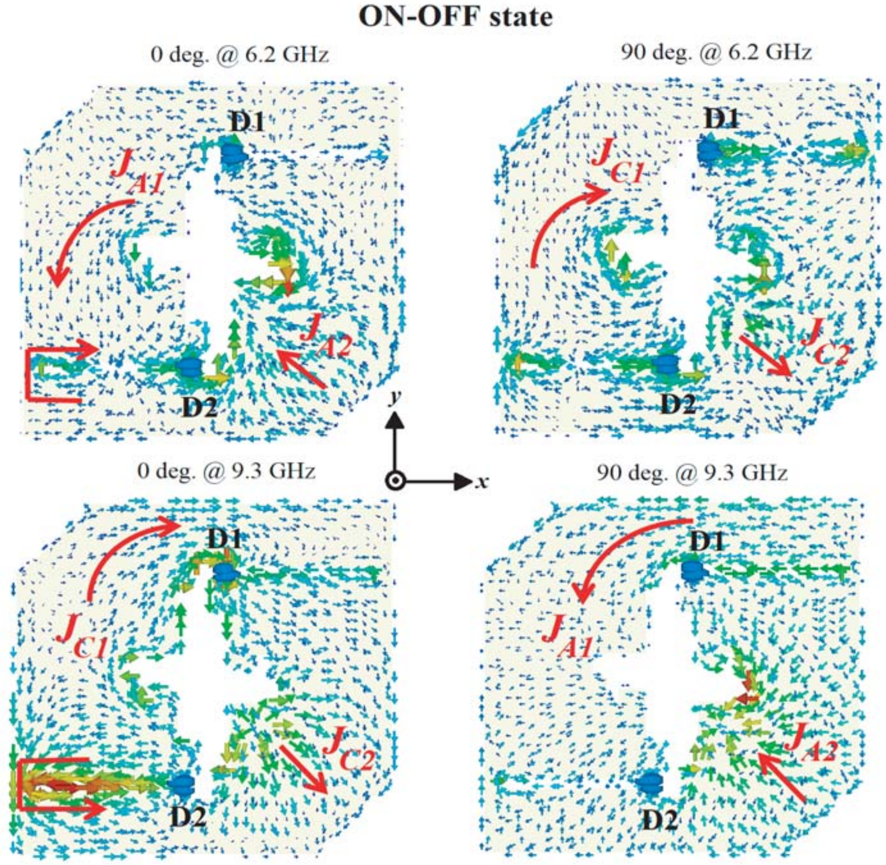

Figure 5. Surface current streamlines at 6.2 GHz and 9.3 GHz for D1-ON, D2-OFF state.

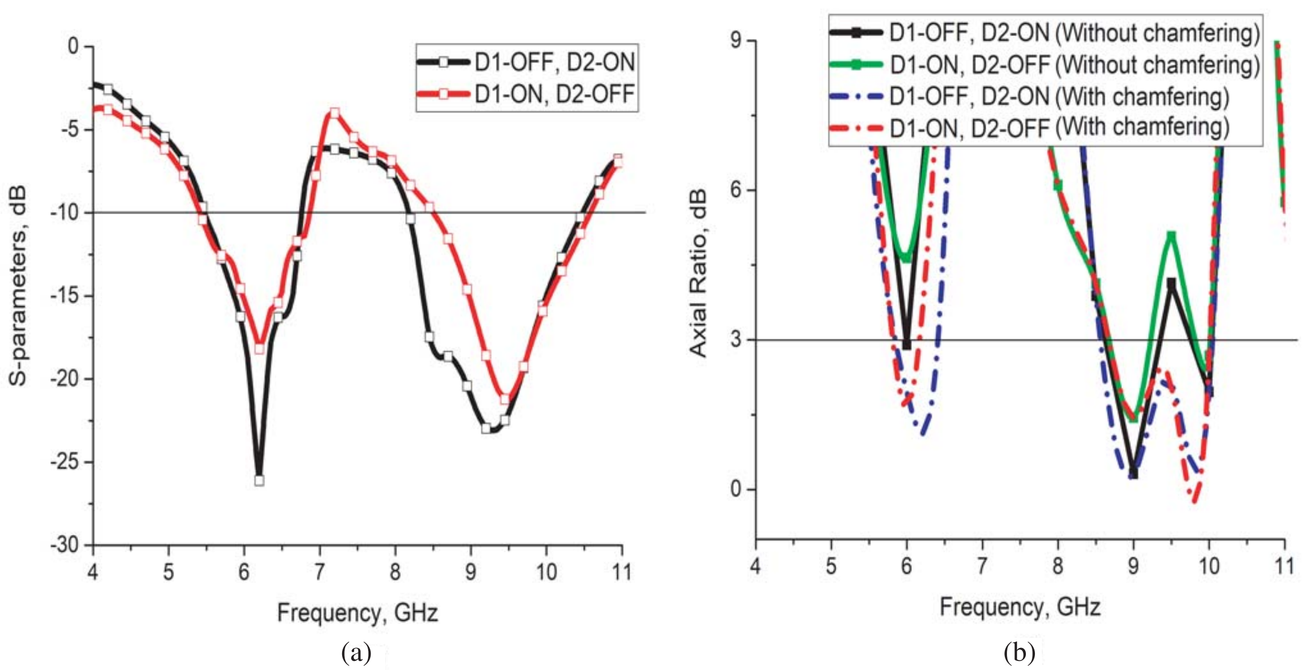

Figure 6. (a) Simulated S-parameters, dB. (b) Axial ratio, dB (with and without chamfering).

4. PARAMETRIC ANALYSIS

A parametric study is conducted by varying the reflector height h_e at different distances from antenna, and S_{11}, dB, and gain, dBi, effects are shown in Figure 7(a) and Figure 7(b), respectively. As we increase h_e, return loss characteristics have deeper responses at lower bands, but bandwidth becomes very narrow, and at higher bands there is a shift in lower resonances. Hence, we fix $h_e = 8.06\,\text{mm}$ as fixed value for good reflection matching characteristics. Similarly, the effect of gain, dBi, is investigated without reflector, which has gain $< 5\,\text{dBi}$ at lower band and $< 6\,\text{dBi}$ at higher band. To optimize antenna gain performance, reflectors at different heights are investigated. To make our design low profile, the reflector is adjusted at an effective height of $\frac{\lambda}{6} \approx 8.06\,\text{mm}$ (λ is the lowest CP frequency), hence lower band gain is increased to 7.82 dBi and higher band gain increased to 8.75 dBi.

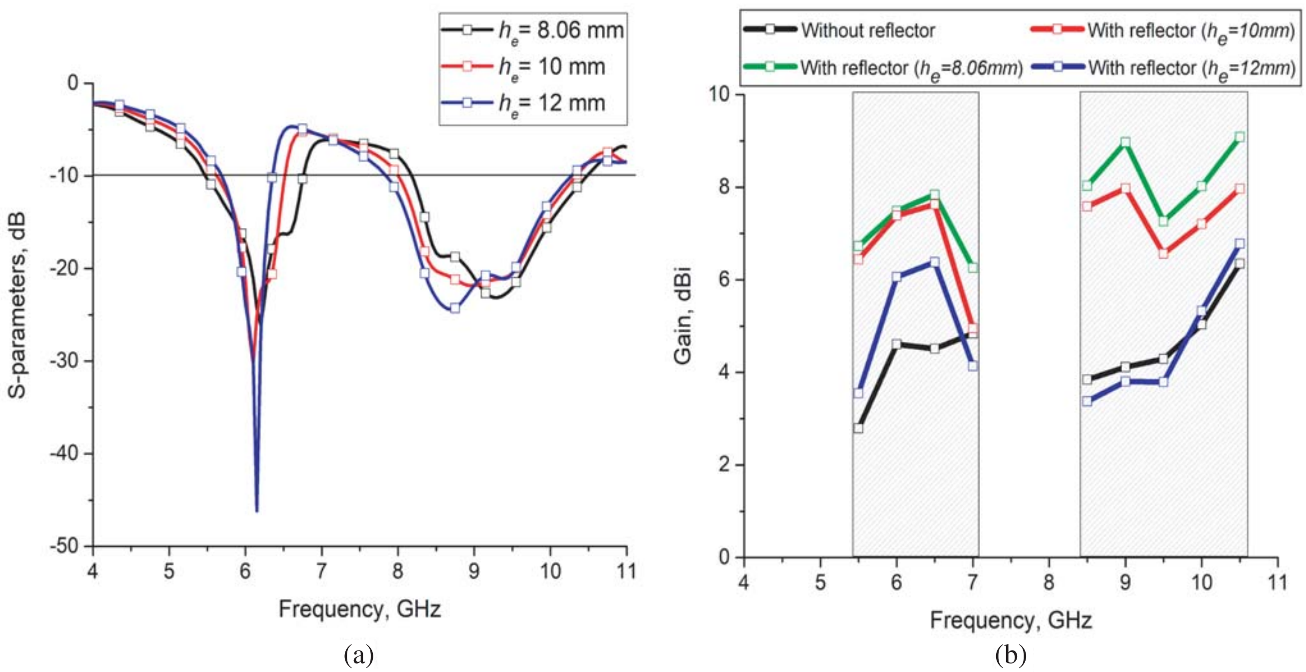

Figure 7. Effects of (a) S-parameters, dB, (b) Gain, dBi in reflector height h_e variation.

The reflector size $L_R \times W_R$ also has an effect on S_{11}, dB, and gain, dBi, responses as shown in Figure 8(a) and Figure 8(b), respectively. When $L_R \times W_R = 30\,\text{mm} \times 30\,\text{mm}$, the center frequency in lower band is shifted to 6.7 GHz, and higher band shows no effect. When the reflector size is increased, the S_{11} response at dual bands is gradually decreased, with no variation at center frequencies. The gain shows a linear variation of (2–5.6 dBi) at lower band and constant variation of (5–6 dBi) at higher band when size ranges from $30\,\text{mm} \times 30\,\text{mm} \leq L_R \times W_R \leq 50\,\text{mm} \times 50\,\text{mm}$. For $L_R \times W_R = 60\,\text{mm} \times 60\,\text{mm}$, the gain is increased by 2.5 dBi at lower band and 2.7 dBi at higher band. In our analysis, optimized height and size of metallic reflector is finally fixed at $h_e = 8.06\,\text{mm}$ and $L_R \times W_R = 60\,\text{mm} \times 60\,\text{mm}$ to achieve maximum gain, stable return loss at dual bands, and sufficient space for cabling connectivity to VNA.

5. EQUIVALENT CIRCUIT

A simplified equivalent antenna circuit model [41] is designed in Advanced Design System (ADS) suite and validated on optimal tuning of lumped elements to match the circuit response with EM-solver. Initially, the circuit modelling requires a conceptual understanding on the cascading R-L-C sets of combinations. Then, the antenna building block conceptualized lumped elements are extracted

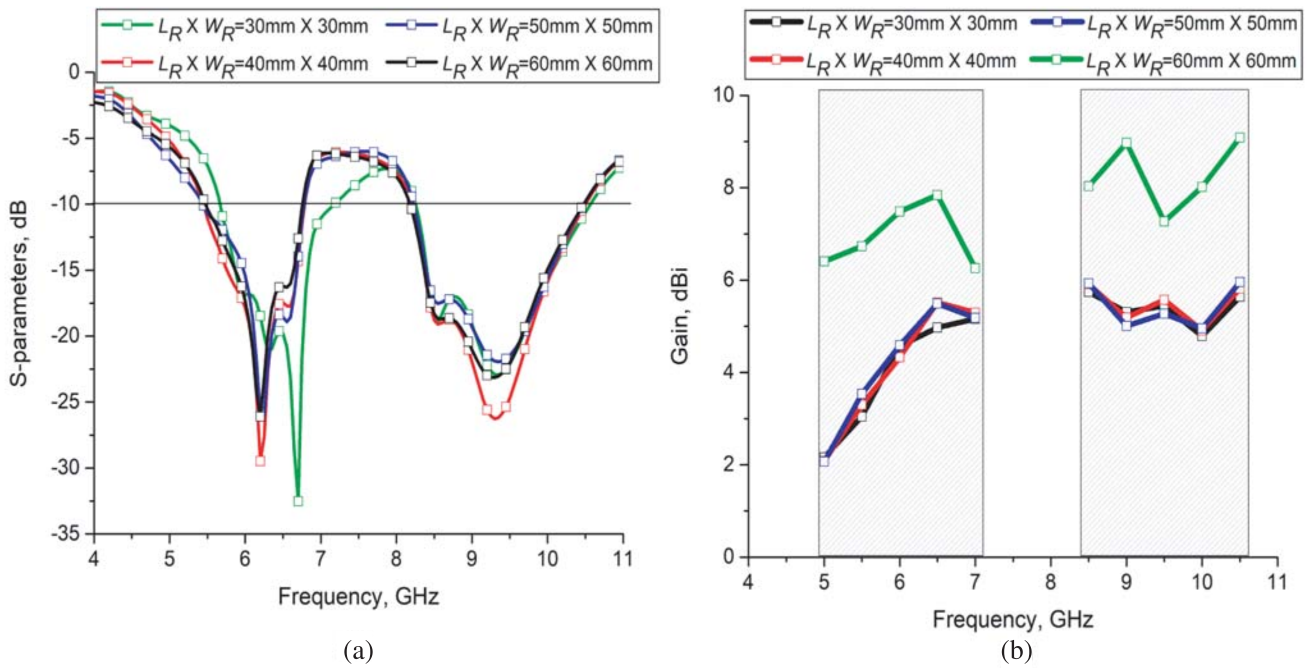

Figure 8. Effects of (a) S-parameters, dB, (b) Gain, dBi in reflector size $L_R \times W_R$ variation.

and calculated by observing impedance characteristics of antenna at dual-bands. Then circuit R-L-C parameters, resonant frequency, B.W. for series and parallel resonance circuit can be estimated from (Q-factor $= \frac{fc}{B.W.}$, where fc = center frequencies of CP bands, and $B.W.$ is the bandwidth of CP bands, $f_c = \frac{1}{2\pi\sqrt{LC}}$, $BW_{Series} = \frac{R}{L}$ and $BW_{Parallel} = \frac{1}{RC}$). The dual-band antenna elements are modelled as R-L-C series (for each resonance) combinations in parallel (for dual-band resonance). Then, parallel-fed R-L-C circuit shown in Figure 9(a) is connected in series to the primitive circuit element to stabilize resonances at lower and higher bands. The equivalent calculated circuit parameters are stated, and the response for dual-bands is shown in Figure 9(b). The metallic reflector acts as an inductive element of lower value to balance the fringing effects of large valued air-gap capacitance and maintain dual-band resonance stability in the equivalent circuit.

6. RESULTS AND DISCUSSIONS

To validate, a prototype antenna is fabricated and measured. The S_{11}, dB, is measured from a PNA series Microwave Network Analyzer (*Model: N5222A*) from Agilent technologies, and radiation patterns are measured in an anechoic chamber.

The measured S_{11}, dB, gain, dBi, and AR, dB for both states are shown in Figure 10(a) and Figure 10(b), respectively. At D1-OFF, D2-ON state, S_{11}, dB, operates from 5.5 to 6.7 GHz with IBW = 19.67% and 8.2 to 10.4 GHz with IBW = 23.66%. The measured axial ratio bandwidths, dB, are 9.20% from 5.7 to 6.25 GHz at the 1st band and 15.63% from 8.55 to 10 GHz at the 2nd band. Similarly, at D1-ON, D2-OFF state, S_{11}, dB, operates from 5.57 to 6.65 GHz with IBW = 17.68% and 8.3 to 10.48 GHz with IBW = 23.21%. The measured axial ratio bandwidths, dB, are 7.53% from 5.75 to 6.2 GHz at the 1st band and 16.04% from 8.6 to 10.1 GHz at the 2nd band. The measured gain responses for D1-OFF, D2-ON state has 7.7 dBi at 6.2 GHz and 8.7 dBi at 9.3 GHz. For D1-ON, D2-OFF state, the gains are 5.87 dBi at 6.2 GHz and 6 dBi at 9.3 GHz. There is a slight discrepancies of measured responses from simulated response, on account of biasing effects, presence of metallic reflector, and cabling effects.

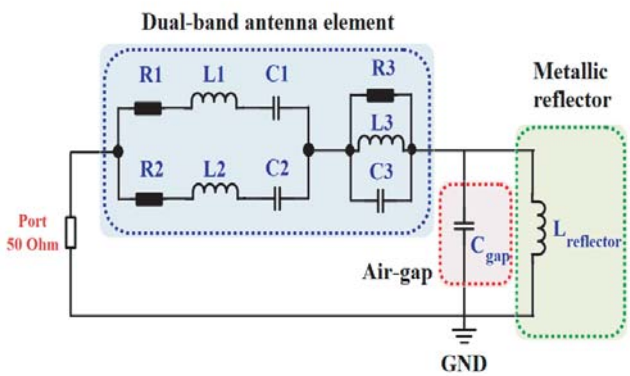

(a)

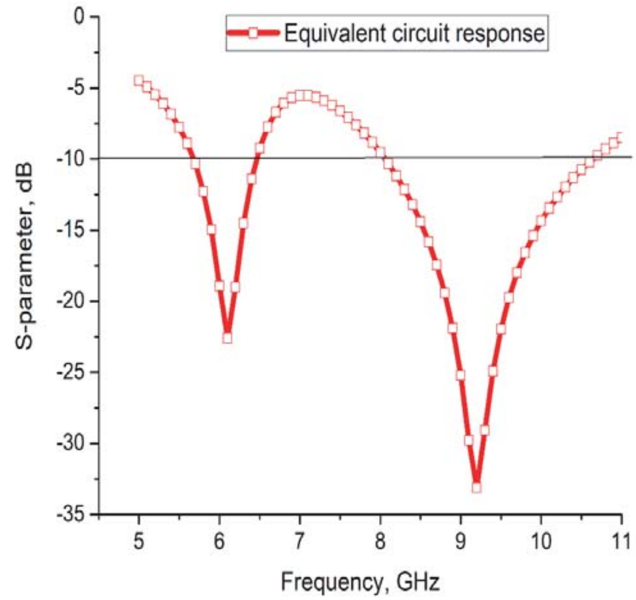

(b)

Figure 9. (a) Equivalent circuit of proposed antenna configuration. (b) Equivalent circuit response. ($Z_0 = 50\,\Omega$, $R1 = 26.3\,\Omega$, $L1 = 7.608\,\text{nH}$, $C1 = 0.0915\,\text{pF}$, $R2 = 23.15\,\Omega$, $L2 = 2.318\,\text{nH}$, $C2 = 0.133\,\text{pF}$, $R3 = 30.5\,\Omega$, $L3 = 8.75\,\text{nH}$, $C3 = 0.098\,\text{pF}$, $L_{reflector} = 0.5\,\text{nH}$, $C_{gap} = 10\,\text{pF}$).

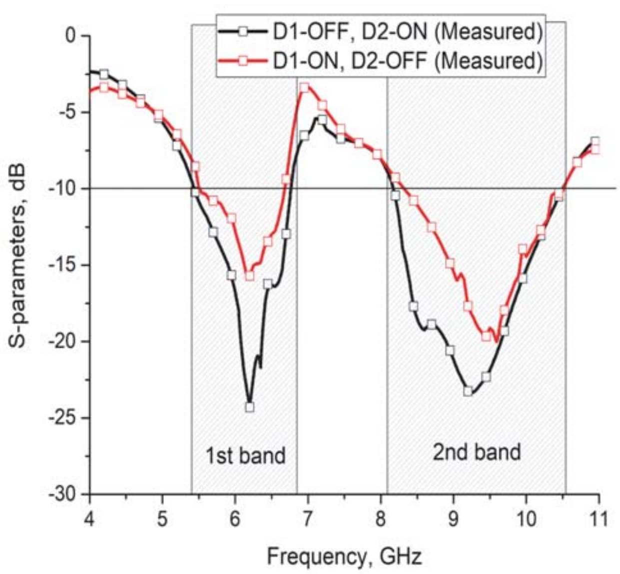

(a)

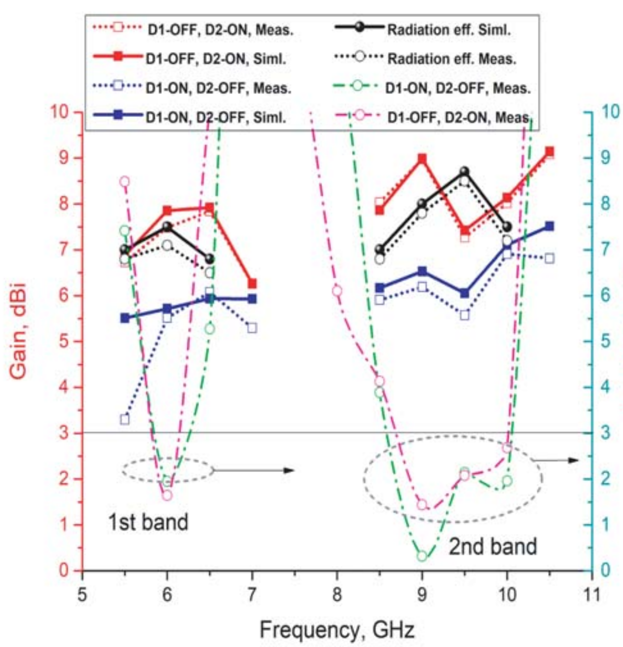

(b)

Figure 10. Validation: Measured (a) S-parameters, dB and (b) Gain, dBi with Axial ratio, dB & Radiation Efficiency, linear scale of proposed antenna.

The simulated and measured radiation plots for D1-OFF, D2-ON states are shown in Figure 11. The dual-polarized behaviour is observed at $\phi = 0°$ and $\phi = 90°$ at 6.2 GHz shown in Figure 11(a) and Figure 11(b), with broadside radiations at $+z$-direction. Similarly, at 9.3 GHz for $\phi = 0°$ and

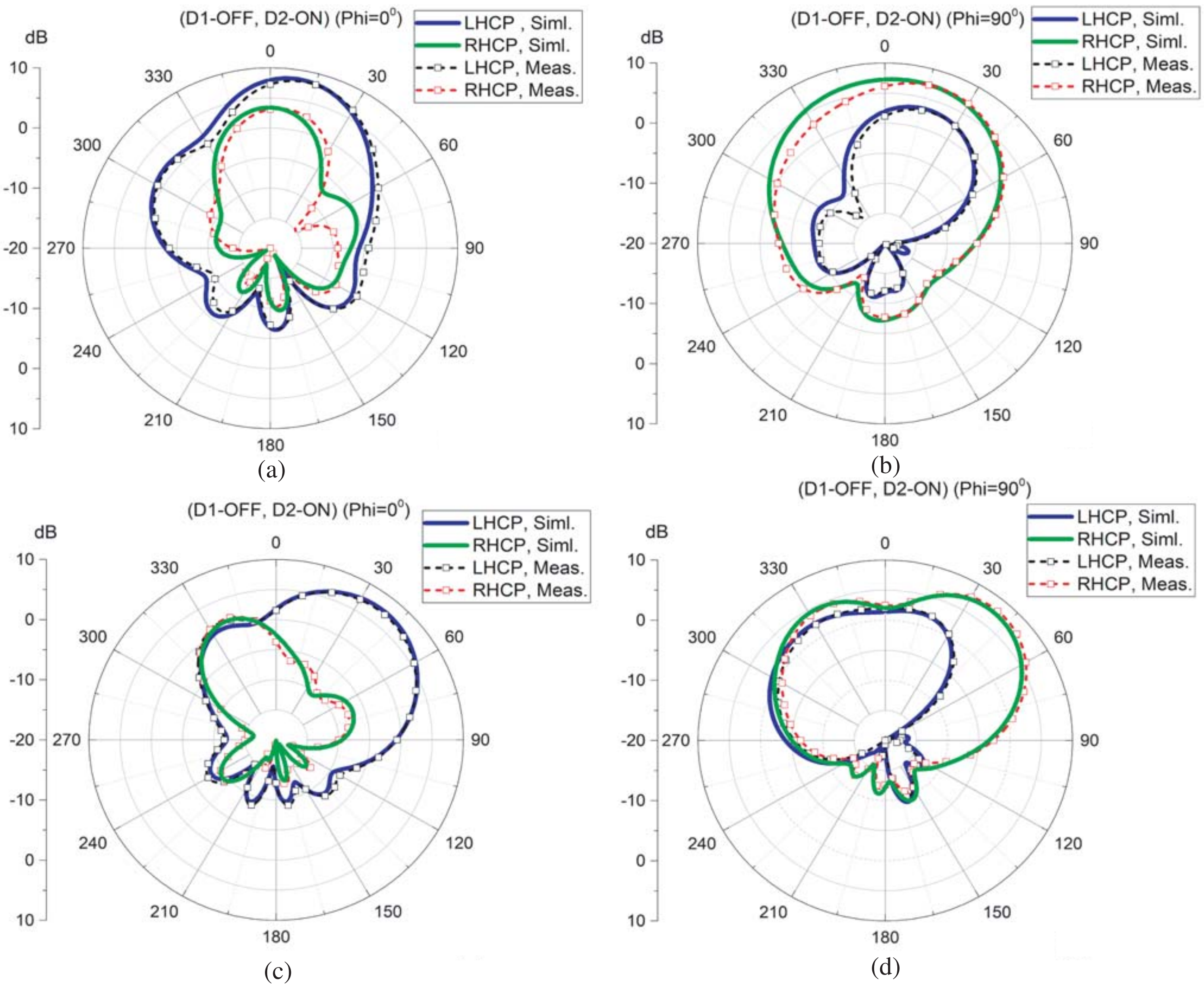

Figure 11. Simulated and Measured radiation patterns for D1-OFF, D2-ON state at (a) 6.2 GHz ($\phi = 0°$), (b) 6.2 GHz ($\phi = 90°$), (c) 9.3 GHz ($\phi = 0°$), (d) 9.3 GHz ($\phi = 90°$).

$\phi = 90°$ shown in Figure 11(c) and Figure 11(d), tilted $\pm 30°$ broadside radiations at $+z$-direction are observed. The tilting of beams account for switching characteristics, which streamlines nonuniform current distributions at the apex of MS, RS, and LS. Due to the metallic reflector back lobe radiations are suppressed by -10 dB at dual bands.

The simulated and measured radiation plots for D1-ON, D2-OFF states are shown in Figure 12. The dual-polarized behaviours are observed at $\phi = 0°$ and $\phi = 90°$ at 6.2 GHz shown in Figure 12(a) and Figure 12(b), with broadside radiations at $+z$-direction. Similarly, at 9.3 GHz for $\phi = 0°$ and $\phi = 90°$ shown in Figure 12(c) and Figure 12(d), tilted $-30°$ broadside radiations at $+z$-direction are observed. From Figure 11 and Figure 12 it is observed that the polarization sense at dual bands is interchanged at $+z$-direction. Hence, it is confirmed that our proposed antenna assists dual-band dual-polarized dual-sense characteristics. The X-pol. level at designated dual-bands is discriminated from Co-pol. which is -10 dB, in the direction of maximum radiation. The radiation efficiency ranges from 75 to 85% at dual bands in both biasing states. Table 3 lists the CP performance analysis on different switching modes. Figure 13(a) shows the fabricated prototype antenna, and Figure 13(b) shows the far-field measurement setup in an anechoic chamber.

The salient features of proposed antenna are:

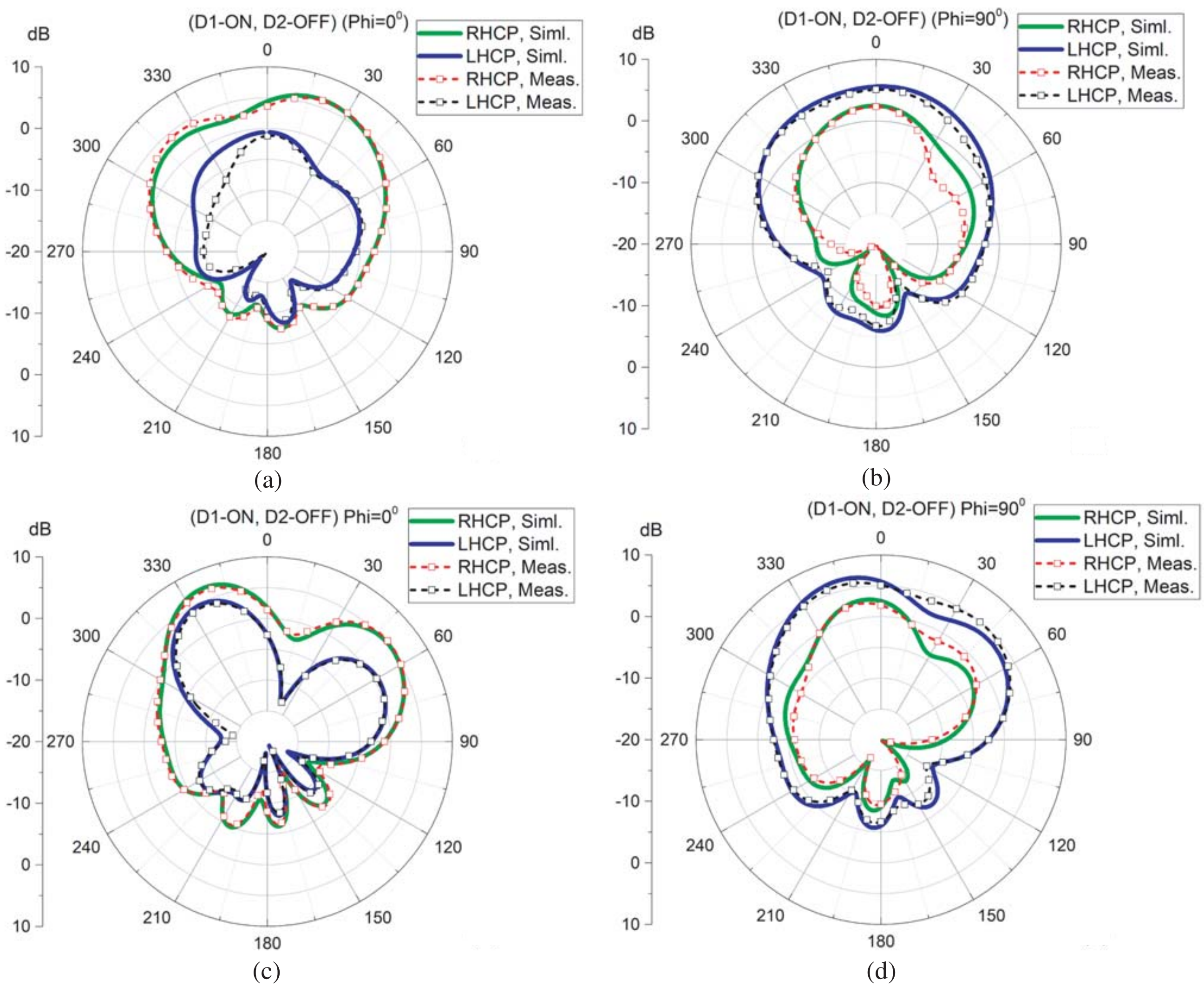

Figure 12. Simulated and Measured radiation patterns for D1-ON, D2-OFF state at (a) 6.2 GHz ($\phi = 0°$), (b) 6.2 GHz ($\phi = 90°$), (c) 9.3 GHz ($\phi = 0°$), (d) 9.3 GHz ($\phi = 90°$).

Table 3. Performance analysis of antenna type on different parameters.

Antenna type	Diode state	Gain_{LB}	Gain_{UB}	ARBW_{LB}	ARBW_{UB}
Without reflector/Dynamic	D1-OFF, D2-ON	4 dBi	4.2 dBi	10.16%	9.94%
Without reflector/Dynamic	D1-ON, D2-OFF	4.5 dBi	5 dBi	12.65%	12.79%
With reflector/Dynamic	D1-OFF, D2-ON	7.7 dBi	8.7 dBi	9.2%	15.63%
With reflector/Dynamic	D1-ON, D2-OFF	5.87 dBi	6 dBi	7.53%	16.04%

Note: — Lower band (LB) — (5.46–6.76) GHz, Upper band (UB) — (8.18–10.48) GHz, ARBW — axial-ratio bandwidth

(a) Low-cost substrate, compact and low-profile, uni-planar printed design.

(b) Antenna design is printed on MS, RS, and LS slot configurations [39, 40]. Polarization is achieved by bridging RF p-i-n diodes, which disturbs the current oscillations in slot configurations, hence, avoiding power-dividers and hybrid couplers.

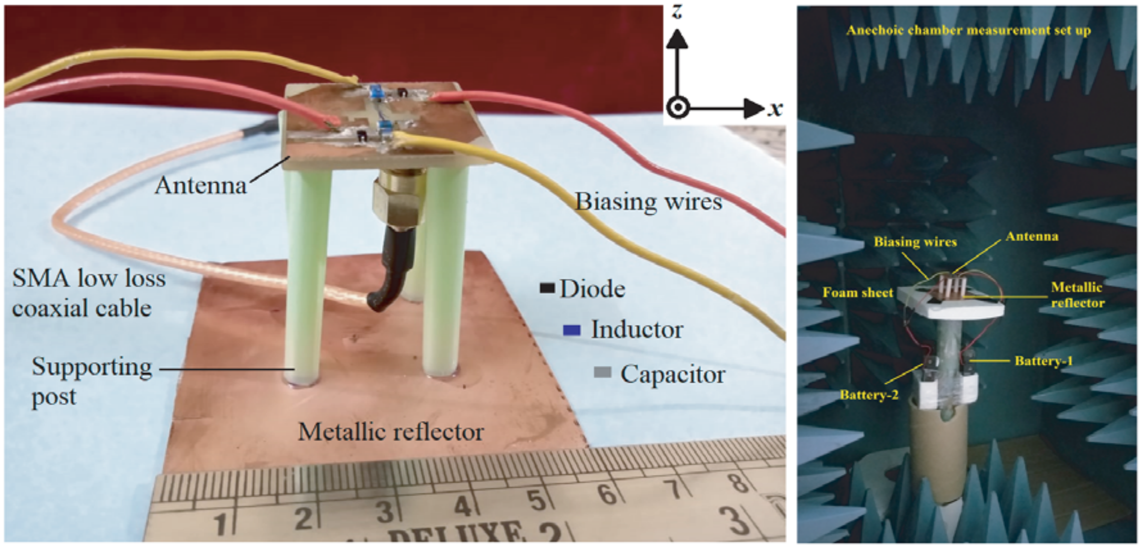

(a) (b)

Figure 13. (a) Fabricated prototype. (b) Antenna measurement set-up in anechoic chamber.

Table 4. Comparision analysis of proposed antenna with other CP antennas.

Ref.	Antenna size	IBW	3-dB Axial BW	Pol. type	CP antenna gain	X-pol.
[5]	60 mm × 55 mm	7.95%	0.33%, 0.72%	DB-DS	5.3 dBi (LHCP) 5.7 dBi (RHCP)	20 dB 15 dB
[6]	112 mm × 112 mm	55.64%	50.99%, 0.72%	DB-DM-DP	1.8 dBi (LB) 8.4 dBi (UB)	15 dB
[7]	40 mm × 40 mm	4.8%, 23%	8.8%	DB-CP	4.3 dBi (LB) 6.4 dBi (UB)	-
[8]	36 mm × 31.2 mm	2.3%, 7.2%	0.6%, 1.4%	DB-DP	4.2 dBi (LB) 6.3 dBi (UB)	20 dB
[9]	38 mm × 32.5 mm	3.93%,29.45%	2.57%	DB-DS	7.7 dBi (LB) 7.4 dBi (UB)	20 dB
[12]	50 mm × 50 mm	0.7%, 5.5%	3.8%, 1.4%	DB-CP	0.8 dBi (LB) 6.8 dBi (UB)	20 dB
[13]	50 mm × 50 mm	111%	55%, 29.3%	DB-DS	4.2 dBi (LB) 3.4 dBi (UB)	15 dB
[14]	112 mm × 112 mm	0.55%, 5.56%	0.56%, 5.09%	DB-CP	3.8 dBi (LB) 4.29 dBi (UB)	20 dB
Pro.	Antenna size 26 mm × 26 mm Reflector size 60 mm × 60 mm	OFF, ON state 19.67%, 23.66% ON, OFF state 17.68%, 23.21%	OFF, ON state 9.2%, 15.63% ON, OFF state 7.53%, 16.04%	DB-DP-DS	OFF, ON state 7.7 dBi (LB) 8.7 dBi (UB) ON, OFF state 5.87 dBi (LB) 6 dBi (UB)	10 dB 10 dB

(Abbreviations: — DB: dual-band, DP: dual-polarized, DS: dual-sense, DM: dual-mode, CP: Circularly polarized, LB: Lower band, UB: Upper band)

(c) The reflectors are fixed at an effective height $\frac{\lambda}{6}$ which asserts high broadside antenna gain.
(d) The biasing mechanism is simple and easy to mount in any RF-interface due to its compactness.
(e) The biasing setup draws minimal power in milli-watts, and the surface mounted electronic elements in proposed design were validated through simulation and experiment, which do not impede antenna performances.
(f) To meet the present day requirements of sub-6 GHz in 5G applications and X-band radar systems, dynamic switched polarization characteristics with electronically switching mechanism is an add-on technical feature.
(g) The sense of polarization, i.e., LHCP and RHCP, can be electronically interchanged depending on RF requirements, which increases the antenna system capacity. The proposed antenna shows dual-band dual-polarized dual-sense behaviour with high gain and stable radiation patterns in both radiation planes.

Table 4 depicts the comparison analysis of proposed antenna with other reported articles. The comparison includes antenna size, impedance bandwidth, 3-dB axial bandwidth, polarization behaviour, CP antenna gain, respectively. The antenna performances are dynamic in nature, where RF signals can be efficiently used owing to their polarization switched behaviour. The present technology can be extended to array antennas using phase shifters, where the relative phases of RF signal carriers can be changed to accomplish beam steerable radiations at different directions. Also the design can be extended to MIMO antennas [37, 38, 43], since excitation of uni-planar slot structure does not require finite ground plane, and can be oriented in different configurations to provide radiation diversity [42] and isolation improvements.

7. CONCLUSION

A dynamically switched dual-band dual-polarized dual-sense compact low-profile uni-planar slot CP antenna is presented. Two RF p-i-n diodes are used to change the polarization sense and behaviour by adopting an electronically switching mechanism. It operates at dual bands (5.46–6.76 GHz) with 21.27% IBW and (8.18–10.48 GHz) with 24.65% IBW for $S_{11} < -10$ dB. By introducing a metallic reflector, high antenna gain is achieved at dual bands, (7.82–8.75 dBi) for D1-OFF, D2-ON state with (9.2%, 15.63%) as axial bandwidths and (6.42–7.0 dBi) for D1-ON, D2-OFF state with (7.53%, 16.04%) as axial bandwidths and radiation efficiency ranging (75–87%). The broadside stable switched polarized radiations with good back lobe suppression makes the antenna system suitable for boresight radiation applications with an aim to reduce polarization mismatch losses. The simulated and measurement results show good agreements on antenna performances. Table 4 highlights that the proposed antenna exhibits better performance with reconfigurable qualifications. Considering the performance attributes, the proposed antenna has the potential to be used for sub-6 GHz in 5G applications or even extended for RF energy harvesting application [44] and X-band radar systems.

REFERENCES

1. Wu, Q., J. Hirokawa, J. Yin, C. Yu, H. Wang, and W. Hong, "Millimeter-wave multibeam endfire dual-circularly polarized antenna array for 5G wireless applications," *IEEE Transactions on Antennas and Propagation*, Vol. 66, No. 9, 4930–4935, 2018.
2. Mao, C., S. Gao, Y. Wang, Q. Chu, and X. Yang, "Dual-band circularly polarized shared-aperture array for C-/X-band satellite communications," *IEEE Transactions on Antennas and Propagation*, Vol. 65, No. 10, 5171–5178, 2017.
3. Chen, Y., Y. Jiao, G. Zhao, F. Zhang, Z. Liao, and Y. Tian, "Dual-band dual-sense circularly polarized slot antenna with a C-shaped grounded strip," *IEEE Antennas and Wireless Propagation Letters*, Vol. 10, 915–918, 2011.
4. Rui, X., J. Li, and K. Wei, "Dual-band dual-sense circularly polarised square slot antenna with simple structure," *Electronics Letters*, Vol. 52, No. 8, 578–580, 2016.

5. Zhao, Z., F. Liu, J. Ren, Y. Liu, and Y. Yin, "Dual-sense circularly polarized antenna with a dual-coupled line," *IEEE Antennas and Wireless Propagation Letters*, Vol. 19, No. 8, 1415–1419, 2020.
6. Cao, W. Q., Q. Q. Wang, B. N. Zhang, and W. Hong, "Capacitive probe-fed compact dual-band dual-mode dual-polarisation microstrip antenna with broadened bandwidth," *IET Microwaves & Antennas Propagation*, Vol. 11, No. 7, 1003–1008, 2017.
7. Chen, K., J. Yuan, and X. Luo, "Compact dual-band dual circularly polarised annular-ring patch antenna for BeiDou navigation satellite system application," *IET Microwaves & Antennas Propagation*, Vol. 11, No. 8, 1079–1085, 2017.
8. Ding, K., C. Gao, Y. Wu, D. Qu, B. Zhang, and Y. Wang, "Dual-band and dual-polarized antenna with endfire radiation," *IET Microwaves & Antennas Propagation*, Vol. 11, No. 13, 1823–1828, 2017.
9. Huang, D. and Z. Du, "Wideband dual-band dual-polarised antenna with less layer radiating patch," *IET Microwaves, Antennas & Propagation*, Vol. 13, No. 8, 1214–1218, 2019.
10. Le, T. T. and H. H. Tran, "Dual-band dual-sense circularly polarized antenna based on crossed dipole structure for WLAN/WiMAX applications," *International Journal of RF and Microwave Computer-Aided Engineering*, Vol. 29, No. 10, e21866, 2019.
11. Mukherjee, S. and A. Biswas, "Design of dual band and dual-polarised dual band SIW cavity backed bow-tie slot antennas," *IET Microwaves, Antennas & Propagation*, Vol. 10, No. 9, 1002–1009, 2016.
12. Wang, M.-S., X.-Q. Zhu, Y.-X. Guo, and W. Wu, "Compact dual-band circularly polarised antenna with omnidirectional and unidirectional properties," *IET Microwaves, Antennas & Propagation*, Vol. 12, No. 2, 259–264, 2017.
13. Xu, R., J.-Y. Li, J. Liu, S.-G. Zhou, K. Wei, and Z.-J. Xing, "A simple design of compact dual-wideband square slot antenna with dual-sense circularly polarized radiation for WLAN/Wi-Fi communications," *IEEE Transactions on Antennas and Propagation*, Vol. 66, No. 9, 4884–4889, 2018.
14. Abdelrahim, W. and Q. Feng, "Compact broadband dual-band circularly polarised antenna for universal UHF RFID handheld reader and GPS applications," *IET Microwaves, Antennas & Propagation*, Vol. 13, No. 10, 1664–1670, 2019.
15. Alibakhshikenari, M., M. Naser-Moghadasi, and R. A. Sadeghzadeh, "Bandwidth and radiation specifications enhancement of monopole antennas loaded with split ring resonators," *IET Microwaves, Antennas & Propagation*, Vol. 9, No. 14, 1487–1496, 2015.
16. Alibakhshikenari, M., M. Naser-Moghadasi, and R. A. Sadeghzadeh, "Composite right-left-handed-based antenna with wide applications in very-high frequency-ultra-high frequency bands for radio transceivers," *IET Microwaves, Antennas & Propagation*, Vol. 9, No. 15, 1713–1726, 2015.
17. Alibakhshikenari, M., S. M. Moghaddam, A. Uz Zaman, J. Yang, B. S. Virdee, and E. Limiti, "Wideband sub-6 GHz self-grounded bow-tie antenna with new feeding mechanism for 5G communication systems," *2019 13th European Conference on Antennas and Propagation (EuCAP)*, 1–4, Krakow, Poland, 2019.
18. Alibakhshikenari, M., B. S. Virdee, and E. Limiti, "Triple-band planar dipole antenna for omnidirectional radiation," *Microwave and Optical Technology Letters*, Vol. 60, No. 4, 1048–1051, 2018.
19. Alibakhshikenari, M., E. Limiti, M. Naser-Moghadasi, B. S. Virdee, and R. A. Sadeghzadeh, "A new wideband planar antenna with band-notch functionality at GPS, Bluetooth and WiFi bands for integration in portable wireless systems," *AEU — International Journal of Electronics and Communications*, Vol. 72, 79–85, 2017.
20. Alibakhshikenari, M., B. S. Virdee, A. Ali, and E. Limiti, "Extended aperture miniature antenna based on CRLH metamaterials for wireless communication systems operating over UHF to C-band," *Radio Science*, Vol. 53, No. 2, 154–165, 2018.
21. Alibakhshikenari, M., M. Naser-Moghadasi, R. A. Sadeghzadeh, B. S. Virdee, and E. Limiti, "A new planar broadband antenna based on meandered line loops for portable wireless communication devices," *Radio Science*, Vol. 51, No. 7, 1109–1117, 2016.

22. Alibakhshikenari, M., M. Naser-Moghadasi, and R. A. Sadeghzadeh, "The resonating MTM-based miniaturized antennas for wide-band RF-microwave systems," *Microwave and Optical Technology Letters*, Vol. 57, No. 10, 2339–2344, 2015.
23. Alibakhshikenari, M. and M. Naser-Moghadasi, "Novel UWB miniaturized integrated antenna based on CRLH metamaterial transmission lines," *AEU — International Journal of Electronics and Communications*, Vol. 69, No. 8, 1143–1149, 2015.
24. Alibakhshikenari, M., M. Movahhedi, and H. Naderian, "A new miniature ultra wide band planar microstrip antenna based on the metamaterial transmission line," *2012 IEEE Asia-Pacific Conference on Applied Electromagnetics (APACE)*, 293–297, Melaka, Malaysia, 2012.
25. Alibakhshikenari, M., B. S. Virdee, and E. Limiti, "Wideband planar array antenna based on SCRLH-TL for airborne synthetic aperture radar application," *Journal of Electromagnetic Waves and Applications*, Vol. 32, No. 12, 1586–1599, 2018.
26. Alibakhshikenari, M., B. S. Virdee, C. H. See, R. Abd-Alhameed, F. Falcone, and E. Limiti, "Array antenna for synthetic aperture radar operating in X and Ku-bands: A study to enhance isolation between radiation elements," *EUSAR 2018 12th European Conference on Synthetic Aperture Radar*, 1–5, Aachen, Germany, 2018.
27. Alibakhshikenari, M., M. Naser-Moghadasi, B. S. Virdee, A. Andújar, and J. Anguera, "Compact antenna based on a composite right/left-handed transmission line," *Microwave and Optical Technology Letters*, Vol. 57, No. 8, 1785–1788, 2015.
28. Alibakhshikenari, M., B. S. Virdee, C. H. See, R. Abd-Alhameed, F. Falcone, and E. Limiti, "Metasurface for controlling polarization of scattered EM waves," *2020 4th Australian Microwave Symposium (AMS)*, 1–2, Sydney, NSW, Australia, 2020.
29. Alibakhshikenari, M., et al., "Mutual coupling reduction using metamaterial supersubstrate for high performance & densely packed planar phased arrays," *2018 22nd International Microwave and Radar Conference (MIKON)*, 675–678, Poznan, Poland, 2018.
30. Alibakhshikenari, M., B. S. Virdee, and E. Limiti, "Compact single-layer traveling-wave antenna design using metamaterial transmission lines," *Radio Science*, Vol. 52, No. 12, 1510–1521, 2017.
31. Alibakhshikenari, M., B. S. Virdee, P. Shukla, C. H. See, R. Abd-Alhameed, M. Khalily, F. Falcone, and E. Limiti, "Antenna mutual coupling suppression over wideband using embedded periphery slot for antenna arrays," *Electronics*, Vol. 7, No. 9, 198, 2018.
32. Zhang, H., Y. Guo, and G. Wang, "A wideband circularly polarized crossed-slot antenna with stable phase center," *IEEE Antennas and Wireless Propagation Letters*, Vol. 18, No. 5, 941–945, 2019.
33. Bhattacharjee, A., S. Dwari, and M. K. Mandal, "Polarization-reconfigurable compact monopole antenna with wide effective bandwidth," *IEEE Antennas and Wireless Propagation Letters*, Vol. 18, No. 5, 1041–1045, 2019.
34. Chen, Q., J. Li, G. Yang, B. Cao, and Z. Zhang, "A polarization-reconfigurable high-gain microstrip antenna," *IEEE Transactions on Antennas and Propagation*, Vol. 67, No. 5, 3461–3466, 2019.
35. Midya, M., S. Bhattacharjee, and M. Mitra, "CPW-fed dual-band dual-sense circularly polarized antenna for WiMAX application," *Progress In Electromagnetics Research Letters*, Vol. 81, 113–120, 2019.
36. Kumar, P., S. Dwari, R. K. Saini, and M. K. Mandal, "Dual-band dual-sense polarization reconfigurable circularly polarized antenna," *IEEE Antennas and Wireless Propagation Letters*, Vol. 18, No. 1, 64–68, 2019.
37. Chaudhary, P., A. Kumar, and B. K. Kanaujia, "A low-profile wideband circularly polarized MIMO antenna with pattern and polarization diversity," *International Journal of Microwave and Wireless Technologies*, Vol. 12, No. 4, 316–322, 2020.
38. Ameen, M., A. Ozair, and R. K. Chaudhary, "Single split-ring resonator loaded self-decoupled dual-polarized MIMO antenna for mid-band 5G and C-band applications," *AEU — International Journal of Electronics and Communications*, Vol. 124, 153336, 2020.
39. Birwal, A., S. Singh, B. K. Kanaujia, and S. Kumar, "CPW-fed ultra-wideband dual-sense circularly polarized slot antenna," *Progress In Electromagnetics Research C*, Vol. 94, 219–231, 2019.

40. Chung, K. L., X. Yan, Y. Li, and Y. Li, "A jia-shaped artistic patch antenna for dual-band circular polarization," *AEU — International Journal of Electronics and Communications*, Vol. 120, 153207, 2020.
41. Mohanty, A. and B. R. Behera, "Investigation of 2-port UWB MIMO diversity antenna design using characteristics mode analysis," *AEU — International Journal of Electronics and Communications*, Vol. 124, 153361, 2020.
42. Koley, S., L. Murmu, and B. Pal, "A pattern reconfigurable antenna for WLAN and WiMAX systems," *Progress In Electromagnetics Research C*, Vol. 66, 183–190, 2016.
43. Kowalewski, J., J. Atuegwu, J. Mayer, T. Mahler, and T. Zwick, "A low-profile pattern reconfigurable antenna system for automotive MIMO applications," *Progress In Electromagnetics Research*, Vol. 161, 41–55, 2018.
44. Behera, B. R., P. Srikanth, P. R. Meher, and S. K. Mishra, "A compact broadband circularly polarized printed monopole antenna using twin parasitic conducting strips and rectangular metasurface for RF energy harvesting application," *AEU — International Journal of Electronics and Communications*, Vol. 120, 15233, 2020.